RSC Publishing Journal of Materials Chemistry A

Anisotropic ^{18}O tracer diffusion in epitaxial films of $GdBaCo_2O_{5+\delta}$ cathode material with different orientations

Journal:	*Journal of Materials Chemistry A*
Manuscript ID:	TA-ART-02-2013-010749
Article Type:	Paper
Date Submitted by the Author:	20-Feb-2013

Complete List of Authors:	Zapata, James; Research Centre for Nanosciencie and Nanotechnology, CIN2 (CSIC/ICN), PLD and Nanoionics Burriel, Monica; Imperial College of London, Garcia, Pablo; Research Centre for Nanosciencie and Nanotechnology, CIN2 (CSIC/ICN), PLD and Nanoionics Kilner, John; Imperial College of Science and Technology and Medicine, Dept of Materials Science Santiso, Jose; Research Centre for Nanosciencie and Nanotechnology, CIN2 (CSIC/ICN), PLD and Nanoionics

Graphical Abstract

Title: Anisotropic ^{18}O tracer diffusion in epitaxial films of $GdBaCo_2O_{5+\delta}$ cathode material with different orientations

Authors: James Zapata, Mónica Burriel, Pablo García, John A. Kilner and José Santiso

Submitted to *Journal of Materials Chemistry A*

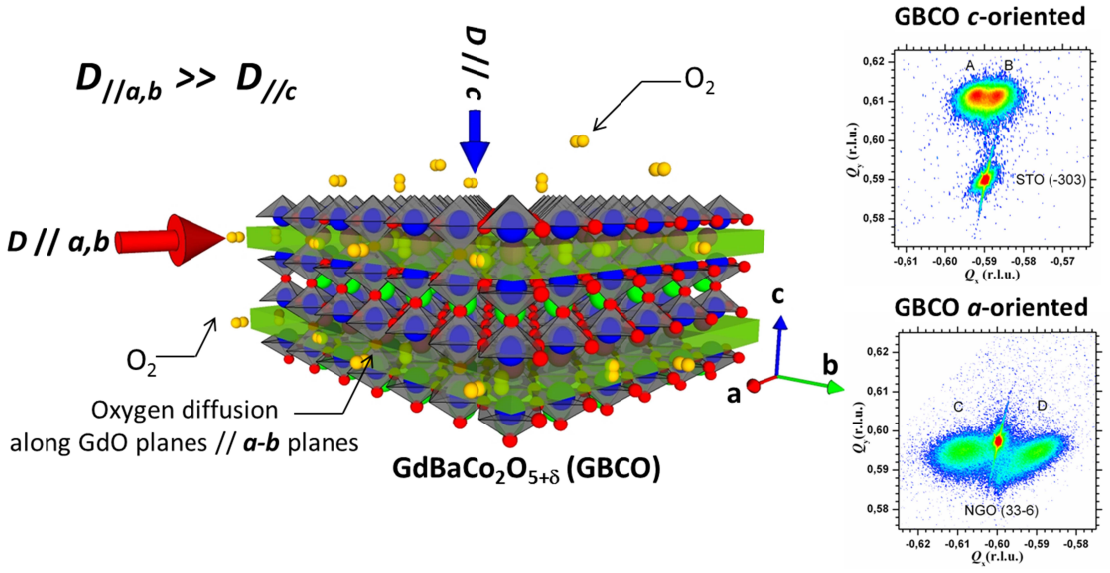

Isotopic ^{18}O tracer diffusion experiments on *c*- and *a*-axis oriented epitaxial thin films of the layered-structure $GdBaCo_2O_{5+\delta}$ (GBCO) compound have directly shown a high degree of anisotropy in the oxygen diffusion coefficient, being one order of magnitude larger along the *a*-*b* plane than along the *c*-axis direction. This fact is essential for engineering high performance textured cathodes in a next generation of Solid Oxide Fuel Cells.

Cite this: DOI: 10.1039/c0xx00000x

www.rsc.org/xxxxxx

ARTICLE TYPE

Anisotropic ^{18}O tracer diffusion in epitaxial films of $GdBaCo_2O_{5+\delta}$ cathode material with different orientations

James Zapata,[a] Mónica Burriel,*[b] Pablo García,[a] John A. Kilner[b,c] and José Santiso*[a]

Received (in XXX, XXX) Xth XXXXXXXXX 20XX, Accepted Xth XXXXXXXXX 20XX

DOI: 10.1039/b000000x

The layered structure of orthorhombic $GdBaCo_2O_{5+d}$ (GBCO) double perovskite compound, currently considered as promising cathode material in Solid Oxide Fuel Cells (SOFCs), is believed to induce a high degree of anisotropy in the oxygen diffusion coefficient, being maximum along the *a*-*b* plane in comparison to the diffusion along the *c*-axis direction. In this study we have deposited films with different orientation: pure *c*-axis and *a*-axis orientation on $SrTiO_3$(001) and $NdGaO_3$(110) single crystals, respectively. The oxygen diffusion was analysed by isotopic ^{18}O exchange depth profiling (IEDP) and Time-of-flight Secondary Ion Mass Spectrometry (ToF-SIMS) in the films along longitudinal and transverse directions at different exchange temperatures and exposure times. The magnitude of longitudinal D^* at low temperatures shows a clear anisotropy. The oxygen diffusion along *a*-axis shows comparable values to bulk polycrystalline GBCO, while it is about one order of magnitude lower along the *c*-axis of the structure. Corresponding oxygen surface exchange rates k^* do not show any anisotropy having comparable values for *c*-axis and *a*–axis orientation. These *k** values are slightly larger than those reported for bulk material showing that thin film textured cathodes may have enhanced activity for oxygen reduction at low temperatures.

Introduction

It is generally believed that one of the limiting steps to reduce the working temperatures of present Solid Oxide Fuel Cell (SOFC) devices is the overpotential caused by the low activity of the cathode reactions, which decreases the performance of the whole device. In this sense there is an intense activity in the quest for active cathode materials which present at the same time large electronic conductivities, high oxygen diffusion and large surface oxygen exchange rates at moderate temperatures. Among the possible compound candidates are perovskite oxides based in substituted $(A,A')(B,B')O_{3\pm\delta}$ with *A*, *A*'= La, Ba, Sr and *B*, *B*'= Co, Fe, as well as oxides with perovskite-related structure members of the Ruddlesden-Popper $A_{n+1}B_nO_{3n+1}$ series, such as $La_2NiO_{4+\delta}$ (*n*=1) and others.[1,2]

Recent work has attracted attention to one of these compounds, namely the double perovskite $GdBaCo_2O_{5+\delta}$ (GBCO), which has shown very high oxygen diffusion coefficients D^* (similar to those of pure ionic conducting materials such as YSZ) and large oxygen surface exchange rates k^*,[3] along with superior chemical stability against typical CeO_2 electrolytes.[4] In this compound Gd and Ba cations alternate in sequential *A*-site layers along the *c*-axis of the structure, whereas Co ions occupy the *B*-sites. The stoichiometric material at standard conditions of pO_2 and *T* holds a substantial oxygen deficiency with oxygen vacancies located mostly on the GdO layers of the structure, parallel to the *a*-*b* plane, and arranged forming channels along the crystallographic *a*-axis [5,6] and δ changing from 0 to 1. This gives rise to a superstructure that doubles along *c* and *b* axis and forms a double perovskite $a \times 2a \times 2a$ cell. The structure of the GBCO material is reported to be orthorhombic *Pmmm* with *a* = 3.862Å, *b*/2 = 3.934Å and *c*/2 = 3.786Å.[6]

The mechanism for the fast oxygen diffusion in this material is reported to involve mainly those oxygen vacancy sites arranged forming parallel channels long the *a*-axis, and is therefore expected to be highly anisotropic, as it has been inferred from molecular dynamics calculations, [7] the oxygen diffusivity being much larger in the *a*-*b* planes of the structure when compared to the diffusivity along the *c*-axis. Therefore, in order to experimentally explore the anisotropic diffusion along different crystallographic directions it is necessary to study either single crystals or highly-textured (epitaxial) thin films. Recent studies on polycrystalline ceramic samples of the praseodymium double perovskite compound $PrBaCo_2O_{5.5}$ have been able to experimentally probe the anisotropy in the oxygen diffusion which is at least four times larger in crystallites with [100] or [010] orientation than in those ones with [001] orientation.[8] The anisotropy value of 4 corresponds to the lower bound for this material, as the measurements were performed on polycrystalline samples with small grain size, and therefore there were experimental limitations associated to inter-grain diffusion and to the random orientation of the grains. Previous attempts to grow epitaxial GBCO films by Pulsed Laser Deposition (PLD) from stoichiometric targets showed a tendency to the formation of Co-deficient films. This induced the generation of planar defects

consisting of supplementary GdO layers, which had an important impact in the charge transport in the films.[9] The purpose of this study is to analyse the oxygen surface exchange and diffusion process on epitaxially grown stoichiometric GBCO films with different orientations With this aim the composition of the PLD target was varied to obtain stoichiometric films. We make use of the ^{18}O tracer diffusion experiments in both longitudinal and transverse directions, using the same methodology as previously described for La_2NiO_4 epitaxial films.[10]

Experimental

Thin films of GBCO were grown by the Pulsed Laser Deposition (PLD) technique using a Compex Pro 201 KrF excimer laser (248 nm) at 10 Hz pulse repetition at a laser fluence of around 3 J/cm^2 (100 mJ in 4.35 mm^2 spot size). The target used was synthesized by conventional solid state reaction using high purity commercial (Alfa Aesar) oxides and carbonates as precursor materials, that is, Gd_2O_3 (99.99%), $BaCO_3$ (99.997%), and Co_3O_4 (99.9985%) oxides (with an excess of 5% cobalt added to compensate the deviations in the cation composition present in layers deposited using a stoichiometric target[7]). After a de-carbonation process at 900 ºC for 20 h the powder was pressed into a circular pellet and annealed over 20 h at 1000 ºC with a final heat treatment at 1250 ºC for 3 h to densify it.

Films about 160 nm thick (which correspond to 4000 ablation pulses) were deposited at substrate temperatures of 850 °C in a 60 mTorr atmosphere of pure O_2 and with the target-substrate distance fixed at about 55 mm. Substrates were commercial single crystals of $SrTiO_3$(001) (STO) and $NdGaO_3$(110) (NGO) (from CrysTec GmbH). After deposition the films were cooled down under the same pO_2 and subsequently investigated by X-Ray Diffraction (XRD) in θ/2θ configuration using a PANalytical X'Pert Pro-MRD instrument (Cu K_α radiation and PIXel detector). The thickness of the GBCO layers was estimated as proportional to the number of pulses after a previous calibration on thinner GBCO films measured by X-ray reflectometry and scanning electron microscope (SEM). For the composition analysis of the films on STO substrate, we used a Cameca SX-50 Microprobe (with four crystal analysers for WDS). The typical voltages used were 12, 15 and 20 keV. A thin film analysis program (STRATAGem) was used to determine the exact composition and thickness of the thin films without interference of the substrate composition.

Film texture along with in- and out-of-plane lattice parameters were accurately determined performing X-Ray reciprocal space maps (RSM) of both film and substrate asymmetric reflections.

The oxygen isotope exchange depth profile (IEDP) technique was used to measure the oxygen surface exchange and diffusion properties of GBCO films in transverse and longitudinal configurations (perpendicular and parallel to the film surface, respectively). The isotopic exchange was carried out at four different temperatures ranging from 300 to 600 °C.

The ^{18}O isotopic exchange experiment was performed under the same equipment and methodology as described in a previous work.[11] In this case the ^{18}O-enriched gas composition was 27.8%. The effective ^{18}O exchange time was calculated taking into account the finite increase/decrease of the sample temperature[12]. In the case of the transverse profiles, the reported surface exchange reaction values were used in the exchanged time correction, since this is the rate-limiting step for oxygen transport in the thin films, while in the case of longitudinal profiles, the corresponding oxygen diffusion values were used.

In order to determine the oxygen transport along the film plane, i.e. longitudinal configuration, a dense and uniform Au thin film of approximately 160 nm was sputtered to cover the GBCO epitaxial film and prevent oxygen exchange from the top surface. A trench was opened at the lateral edge of the film, allowing the exchange with the ^{18}O enriched exchange gas phase and thus ensuring the diffusion of the ^{18}O species only along the direction parallel to the film plane.[10]

All the exchanged samples were measured by time-of-flight secondary ion mass spectrometry (ToF-SIMS) on a Ion ToF-SIMS 5 machine (ION-TOF GmbH, Münster, Germany) equipped with bismuth LMIS pulsed gun incident at 45°. A 25 kV Bi^+ primary ion beam was used to generate the secondary ions using the low mass resolution or burst alignment mode (eight pulses) for analysis and a Cs^+ beam (2 kV) incident at 45° for sputtering. For the longitudinal configuration secondary ion images for selected areas of the GBCO film, including the edge of the opened trench, were acquired. For the transverse configuration (perpendicular to the film plane) tracer oxygen depth profiles were measured from the exchanged surface penetrating down to the substrate by sputter depth profiling.

Results and Discussion

Film Orientation

Figures 1(*a*,*b*) show typical X-ray diffraction patterns obtained for GBCO films grown at a fixed oxygen partial pressure pO_2 of 60 mTorr and 850 ºC on STO(100) and NGO(110) substrates, respectively. On STO the patterns show one set of 00*l* GBCO reflections with out-of-plane parameter of about 3.775 Å, consistent with the *c*/2 value of the bulk GBCO material. The presence of intense reflections in the intermediate positions between main substrate reflection (indexed as *l*=odd) is also characteristic of the GBCO double perovskite superstructure arising from the Gd/Ba sequential A-site arrangement in the [001] direction. No additional peaks corresponding to other phases or orientations appear under these deposition conditions. Therefore, the films on STO correspond to purely *c*-axis oriented GBCO. This texture was also confirmed by the reciprocal space maps around the -303 STO reflection (Figure 1.c). The map shows a film reflection at Q_y= 0.6122 r.l.u. (reciprocal lattice units) of GBCO, corresponding to an out-of-plane parameter *c*/2 = 3.77(1) Å, in good agreement with the value obtained from the θ/2θ scans. The elongated shape of the peak in the horizontal direction defines two distinct maxima (labeled *A* and *B* in the map), which were attributed to the incipient *a*/*b* differentiation of the orthorhombic phase. Their corresponding in-plane parameter values are 3.89(1) Å for ***A*** and 3.92(1) Å for ***B***. These values are slightly larger and shorter than the corresponding *a* = 3.862 Å and *b*/2 = 3.934 Å, respectively, reported for the bulk phase,[6] and are therefore assigned to these crystallographic directions indicating a certain degree of biaxial in-plane strain, tensile along *a*-axis and compressive along *b*-axis.

Standard θ/2θ XRD patterns of the films deposited on NGO

(110), Figure 1.b, do not show clearly differentiated film peaks, only a weak shoulder at the larger angle side of the 110 substrate peak (equivalent to 001 reflection for the primitive cubic cell) was observed.

Reciprocal space maps around the 33-6 NGO reflection (equivalent to -303 reflection for the primitive cubic cell), shown in Figure 1.d, evidence the presence of two clear contributions, labeled *C* and *D*, at common Q_y position. This corresponds to an out-of-plane parameter of 3.86(1) Å, very close to the *a*-axis parameter of the bulk phase. The coincidence of this value with that of the NGO substrate explains why the GBCO peaks are not observed in the standard patterns, since they perfectly overlap with the NGO peaks. The corresponding in-plane parameter values for *C* and *D* are 3.815 Å and 3.925 Å, respectively, these values being slightly longer (and shorter) than those corresponding to *c*/2 (and *b*/2) of bulk GBCO phase. This indicates pure *a*-axis orientation perpendicular to the film, and coexisting *c*- and *b*-axis parallel to main in-plane [100]/[010] crystallographic orientations of the substrate primitive cell. Figure 1.e and 1.f show the schemes of the relative orientations of film and STO and NGO substrates, respectively. As in the case of *c*-axis oriented films on STO, pure *a*-axis oriented films on NGO show a certain degree of biaxial strain. Table I collects the calculated mismatch between film and substrate cells for the different orientations as well as the measured cell parameters on both STO and NGO substrates. Mismatch calculations involving orthorhombic structures may become confusing if one compares the linear differences between cell parameters for each crystallographic orientation (two cell parameters for each pseudocubic <100> orientation). Instead, a simpler approach consists of comparing the area mismatch between the corresponding rectangular sides of each primitive cell with the plane cut of the substrate. As an example, the mismatch for the GBCO *a*-axis oriented domains on NGO is calculated by comparing the areas of the rectangular plane cut of the substrate: $a' \times b' = 3.864 \times 3.855 = 14.896$ Å^2, and the rectangular plane formed by GBCO $b/2 \times c/2 = 3.934 \times 3.786 = 14.894$ Å^2. Their difference ($Area_{film}$ - $Area_{subs}$)/ $Area_{subs}$ is -0.02% (slightly compressive), as depicted in table 1. This also helps to realize that even though the direct comparison of the separate cell parameters may induce an uniaxial strain of opposite sign along the two in-plane directions ($a'<c/2$, $b'>b/2$) the area mismatch is very small. Therefore it is not surprising that the corresponding GBCO out-of-plane value is not very different to the bulk value (less than +0.1% difference). By comparing the different film-substrate orientations the lower mismatch area was clearly obtained for *c*-axis orientation on STO and *a*-axis orientation on NGO, in good agreement with the experimental observation.

(insert Table 1 here)

Occasionally, in some of the films deposited on NGO substrates, a certain amount of *c*-axis oriented domains (very weak peaks) were observed depending on the deposition conditions. This indicates that growth of GBCO on this substrate is much more sensitive to subtle changes in the deposition parameters.

Despite some subtle differences in their strain, we may conclude that depending on the substrate type the films are purely *c*-axis and predominantly *a*-axis oriented on STO and NGO substrates, respectively. Since in GBCO *Pmmm* structure the fast oxygen migration path would follow the crystallographic *a*-axis, it would be expected that depending on the film orientation the films may behave in a very distinct way. In films with *c*-axis orientation their corresponding crystallographic *a*-axis lays parallel to both main in-plane directions, while in *a*-axis oriented films is perpendicular to the film.

The average cationic composition measured by WDS microprobe analysis of the films deposited on STO (001) from the Co-enriched (5%) target corresponded to 0,96:1,02:2,02. This corrected the observed Co-deficient films observed in films deposited by PLD from stoichiometric 1:1:2 ([Gd]+[Ba])/[Co]=1) targets which induced the formation of a large density of planar defects.[10]

Oxygen surface exchange in transverse geometry

The oxygen transport along the transverse direction (perpendicular to the film plane) for the GBCO thin films was determined from the depth profiles obtained with the IEDP technique in combination with ToF-SIMS analysis. Figures 2*a* and *b* show the corresponding normalized ^{18}O isotopic oxygen fraction for the different exchange temperatures, on STO and NGO substrates, respectively. Figure 2.c shows a scheme of the measuring geometry.

The calculation of the oxygen transport parameters is achieved by fitting the experimental data to the appropriate solution of the diffusion equation. We assume for this configuration the model of an infinite solid slab extending over the region of thickness *2l* in which the initial isotope fraction is C_{bg} and the diffusion anneal takes place in a large volume of gas of constant isotope fraction C_g. The symmetrical solutions given by this plane sheet model (x being the distance from the film–substrate interface, and l the film thickness) occupying the region $-l<x<l$, apply also to the sheet $0<x<l$ when the face $x = 0$ is non-permeable. The solution to the diffusion equation given by Crank[13] is as follows:

$$c_r(x,t) = \frac{C(x,t) - C_{bg}}{C_g - C_{bg}} = 1 - \sum_{n=1}^{\infty} \frac{2L\cos(\beta_n x/l)\exp\left(-\beta_n^2 D^* t/l^2\right)}{\cos\beta_n(\beta_n^2 + L^2 + L)} \qquad (1)$$

Where $C(x, t)$ is the ^{18}O isotope fraction obtained by SIMS, *i.e.* $^{18}O/(^{18}O+^{16}O)$, t is the time of the isotope exchange, D^* is the oxygen tracer diffusion coefficient; k^* is the surface tracer exchange coefficient and β_n ($n=1, 2, \ldots$) are the nonnegative roots of $\beta \tan \beta = L$, and $L = l \cdot k^*/D^*$ The limitations of the technique are examined in detail elsewhere.[14-17]

The profiles are almost flat across the film thickness down to the interface with the substrate. This indicates that oxygen diffusion is too fast to be measurable for the current film thickness at the exchange conditions (T and t), so the rate-limiting step in this geometry is the oxygen surface exchange. No information about diffusion was extracted for this geometry and thus only tracer exchange rates k^* were obtained. Fig. 3 depicts an Arrhenius plot

of the corresponding *k** values, obtained for the best fit of the experimental data to the diffusion equation solution, eqn (1), along with those values reported in literature at similar *T*. For the low temperature region, the oxygen surface exchange rates for both film orientations are about half order of magnitude larger than those reported for bulk material, with similar activation energies, while the bulk and thin film values are comparable at the high temperatures. The larger surface activities at low temperatures could be due to the textured films whose surface predominantly expose particular crystallographic planes, (001) or (100) for pure ***c***- or ***a***-axis oriented films, respectively. This indicates a greater potential for thin films with controlled surface orientation as cathodes for SOFC application at intermediate operation temperatures. The comparison between the films indicates that regardless their texture, films with *c*- or *a*-axis orientation show comparable surface activity for oxygen exchange. Either there are little differences in the surface chemical termination, or the possible differences in the surface termination plane (presumably of pure *A*O or *A*'O planes for pure *c*-axis oriented films or mixed *A*O/*A*'O in the case of pure *a*-axis oriented films) do not play an important role in oxygen exchange. However, the slight reduction observed at higher temperatures might be due to a surface atomic rearrangement induced by the long annealing times under pure O_2 atmosphere needed for the anneal step prior to the ^{18}O exchange, which might cause surface segregation, as observed in Sr-substituted $LaCoO_3$ [18] as well as in $La_{0.8}Sr_{0.2}MnO_3$ perovskite.[19]

Oxygen surface exchange and diffusion in longitudinal geometry

Figures 4*a* and *b* show longitudinal concentration profiles obtained for the films deposited on STO and NGO substrates at three different temperatures. For fitting the longitudinal concentration profiles the semi-infinite medium solution of the diffusion equation was used.[13] For this particular geometry, the analysis provides both the oxygen exchange, *k**, and diffusion coefficients, *D**, along the plane of the film, which correspond to different crystallographic orientations according to the film texture, i.e. along *a/b* direction for *c*-axis oriented films on STO, and along *b/c* direction on *a*-axis oriented films on NGO. The solution to the diffusion equation can be written in terms of the dimensionless parameters and as $\boldsymbol{x' = x / \sqrt{4D^* t}}$ and $\boldsymbol{h' = (/D^*)\sqrt{4D^* t}}$ as

$$\boldsymbol{c_r(x,t) = \frac{C(x,t) - C_{bg}}{C_g - C_{bg}} =}$$

$$\boldsymbol{erfc(x') - exp\left(2h'x' - h'^2\right) erfc(x' + h')} \quad (2)$$

*D** and *k** values obtained for the measured regions of the exchanged samples are depicted in the Arrhenius plots in Figure 5 *a* and *b*. Despite the inherent variability in the measurement of *k**, the values for this longitudinal geometry follow a similar trend to the one observed in the transverse geometry. The surface exchange coefficients for films on STO and NGO (Fig 5.a) show values from half to one order of magnitude larger than the bulk ones, and are slightly larger than those reported for transverse geometry. This could be related to a higher activity of the freshly cut trenches opened in this experiment in comparison with the top film surface more exposed to surface contamination and degradation in the case of transverse geometry. Besides, this longitudinal configuration may be less affected by surface segregation during the low temperature anneal because of the particular geometry and the surface-to-volume ratio and, therefore, remain more active for oxygen reduction. Again, there are no significant differences related to film orientation, as it would be expected in this case since the exposed surfaces very likely consist of a combination of different crystallographic planes, *i.e.*: (100)/(010) for the *c*-axis oriented films on STO, and (001)/(010) for the *a*-axis oriented films on NGO.

The most remarkable differences are observed in the *D** tracer diffusion coefficient, in Fig. 5b. While the *D** values obtained on *c*-axis oriented GBCO/STO are slightly higher than the reported bulk material in the full range of temperatures, those obtained on *a*-axis oriented GBCO/NGO deviate substantially, being almost one order of magnitude smaller in the low temperature range between 300 and 400 ºC. For pure *c*-axis oriented films the diffusion path in the longitudinal geometry is parallel to the ***a/b*** crystallographic planes, and therefore the measured ***D**** values are taken as the maximum intrinsic values. On the other hand, in a pure *a*-axis oriented film there would be *a/b* planes perpendicular to the diffusion path, but also parallel due to the mixed *b* and *c* orientation within the film plane. Depending on the grain connectivity, there is little chance for a direct diffusion path along *a*-*b* planes, as in the case of *c*-axis oriented films. Therefore, the observed reduction of the tracer diffusion coefficient *D** is evidence of the diffusion anisotropy, as has also been proven in polycrystalline samples of $PrBaCo_2O_{5.5}$. For this material the diffusion coefficient was found to be larger in the [100]/[010] direction compared to [001].[6] At the highest temperature the *a*-axis oriented film shows comparable *D** value to the *c*-axis oriented and bulk values. It cannot be ruled out that the presence of a small amount of *c*-axis orientation in predominantly *a*-axis oriented samples, as could be the case for this particular sample, might provide a fast diffusion path and therefore a substantial increase in the diffusion coefficient. If that was the case the anisotropy in GBCO may be even of a larger magnitude and therefore the largest anisotropy value measured (one order of magnitude) constitutes the lower bound of the measurements taking into account the possible fast diffusion paths through grain boundaries or regions with different orientation. The fact that *D** values along the fastest diffusion direction are similar to those reported for polycrystalline GBCO material (with a random distribution of domain orientations) indicates that the bulk material presents a substantial connectivity between *a/b*-planes so the fastest diffusion path dominates, which reinforces the suitability of these ordered perovskites for MIEC cathodes.

4. Conclusions

We have deposited high quality epitaxial films of the mixed ionic-electronic conducting material $GdBaCo_2O_{5.5+\delta}$ on different substrates, and demonstrated that the appropriate choice of substrate mismatch allows growing films with either pure *c*-axis

or *a*-axis orientation. This has allowed exploration of the potential anisotropy in the oxygen transport and has proven that indeed the oxygen diffusion at low temperatures is almost one order of magnitude larger along *a*-axis compared to *c*-axis. This has been related to the arrangement of oxygen vacancies preferentially in the GdO planes forming channels along the *a*-axis, and therefore providing a path for oxygen migration. However, no influence of the structure anisotropy was observed in the oxygen surface exchange rates, which were of similar values regardless the film orientation or measuring geometry. The method described here provides a very powerful tool to explore intrinsic oxygen transport properties in complex anisotropic oxide materials otherwise dominated by the mixture of all orientations and grain boundary contributions in polycrystalline samples.

Acknowledgements

The authors would like to acknowledge the Spanish Ministry of Education and Culture for financial support (MAT2011-29081-C02-01 and CONSOLIDER-INGENIO CSD2008-0023 projects). This research was also supported by a Marie Curie Intra European Fellowship within the seventh European Community Framework Programme (PIEF-GA-2009-252711) (for M.B). J. Z. thanks the Spanish National Research Council (CSIC) for JAE-PreDoc Scholarship. The authors would like to thank Dr. S. Fearn and R. Charter for their help with ToF-SIMS analysis.

Notes and references

[a] *Centro de Investigación en Nanociencia y Nanotecnología, CIN2 (CSIC-ICN), Campus UAB. 08913 Bellaterra. Barcelona. Spain. Tel: +34 93 5814700; E-mail: jsantiso@cin2.es*

[b] *Department of Materials, Imperial College London, London SW7 2AZ, UK. E-mail:m.burriel@imperial.ac.uk*

[c] *International Institute for Carbon Neutral Energy Research,744 Motooka, Nishi-ku Fukuoka 819-0395, Japan*

† Electronic Supplementary Information (ESI) available: [details of any supplementary information available should be included here]. See DOI: 10.1039/b000000x/

‡ Footnotes should appear here. These might include comments relevant to but not central to the matter under discussion, limited experimental and spectral data, and crystallographic data.

1 A. Tarancón, M. Burriel, J. Santiso, S.J. Skinner, J. A. Kilner, *J. Mater. Chem.* 2010, **20**, 3799–3813.

2 J. Santiso and M. Burriel, *J. Solid State Electrochem*., 2011, **15**, 985-1006.

3 A. Tarancón, S. J. Skinner, R. J. Chater, F. Hernández-Ramírez and J. A. Kilner, *J. Mater. Chem*., 2007, **17**, 3175-3181.

4 A. Tarancon, J. Pena-Martinez, D. Marrero-Lopez, A. Morata, J. C. Ruiz-Morales and P. Nunez, *Solid State Ionics*, 2008, **179**, 2372-2378.

5 A. Maignan, C. Martin, D. Pelloquin, N. Nguyen and B. Raveau, *J Solid State Chem.*, 1999, **142**, 247-260.

6 C. Frontera, J. L. Garcia-Munoz, A. Llobet and M. A. G. Aranda, *Phys. Rev. B*, 2002, **65**, 180405(R).

7 D. Parfitt, A. Chroneos, A. Tarancon and J. A. Kilner, *Journal of Materials Chemistry*, 2011, **21**, 2183-2186.

8 M. Burriel, J. Pena-Martinez, R. J. Chater, S. Fearn, A. V. Berenov, S. J. Skinner and J. A. Kilner, *Chem. Mater*., 2012, **24**, 613-621.

9 M. Burriel, M. Casas-Cabanas, J. Zapata, H. Tan, J. Verbeeck, C. Solís, J. Roqueta, S. J. Skinner, J. A. Kilner, G. Van Tendeloo, and J. Santiso, *Chem. Mater.*, 2010, **22**, 5512-5520

10 M. Burriel, G. Garcia, J. Santiso, J. A. Kilner, J. C. C. Richard and S. J. Skinner, *J. Mater. Chem.*, 2008, **18**, 416-422.

11 J. A. Kilner, B. C. H. Steele and L. Ilkov, *Solid State Ionics*, 1984, **12**, 89.

12 D. R. Killoran, *J. Electrochem. Soc*. 1962, **190**, 170−171

13 J. Crank, The Mathematics of Diffusion, *Oxford University Press*, Oxford, 1975.

14 R. A. De Souzaand R. J. Chater, *Solid State Ionics*, 2005, **176**, 1915,

15 R. A. De Souza and M. Martin, *MRS Bulletin*,2009, **34**, 907-914.

16 E. Fischer and J. L. Hertz, *Solid State Ionics*, 2012, **218**, 18–24.

17 F. Ciucci, *Solid State Ionics*, 2013, **232**, 97-105.

18 Z. Cai, M. Kubicek, J. Fleig, and B. Yildiz, *Chem. Mater*., 2012, **24**, 1116–1127.

19 S. Fearn, J. C. H. Rossiny, J. A. Kilner and J. R. G. Evans, *Solid State Ionics* 2012, **211**, 51-57.

20 K. Momma and F. Izumi, *J. Appl. Crystallogr.*, 2011, **44**, 1272-1276.

Figure captions

Fig. 1. XRD patterns of GBCO films deposited at 850 ºC by PLD on STO (001) (*a*) and NGO (110) (*b*) substrates. STO is cubic while NGO is orthorhombic. However both orientations correspond to (100) plane cut of pseudocubic primitive cell. Intense substrate peaks are labelled with asterisks (STO) and triangles (NGO). Films on STO (*a*) show (00*l*) reflections corresponding to *c*-axis oriented GBCO superstructure with double cell parameter (*c*/2= 3.77(1) Å) associated to the Gd/Ba order. On NGO (110) (*b*) the patterns only show a weak contribution close to the substrate peaks. Reciprocal space maps of those films on STO (*c*) and NGO (*d*) in the area of the pseudocubic primitive -303 reflection (33-6 for the NGO) reveal the orientation of GBCO film being *c*-axis oriented on STO and *a*-axis oriented on NGO. In both cases the split peak along Q_x is consistent with *a*- and *b*-parameters (for *c*-axis oriented GBCO/STO, labelled *A* and *B*, respectively) and *c*- and *b*- axis (for *a*-axis oriented GBCO/NGO, labelled *C* and *D*) of strained orthorhombic GBCO structure. The schemes in (*e*) and (*f*) depict the corresponding epitaxial orientation between film and substrate on STO and NGO, respectively. (Models have been generated using Vesta software.[20] Coloured spheres in GBCO correspond to Gd, purple, and Ba, green, while Sr is green and Nd is golden in STO and NGO, respectively)

Fig. 2. Normalised ^{18}O isotope fraction along the transverse direction (depth profile) of GBCO films of about 160 nm thickness deposited on STO (*a*) and NGO (*b*) at exchange temperatures of 328, 384 and 463 ºC, and times of 544, 883 and 630 s, respectively. The scheme (in *c*) depicts the experimental arrangement for the ^{18}O exchange directly through the top film surface.

Fig. 3. The oxygen surface exchange rates (k^*) plotted as a function of reciprocal temperature for the GBCO films with *c*- and *a*-axis orientation (deposited on STO and NGO, respectively). The graph also includes values for bulk GBCO ceramic from the literature.[3] The dashed lines are only a guide to the eye.

Fig. 4. Normalised isotopic fraction profile along the longitudinal direction of the *c*-axis (a) and *a*-axis (b) GBCO oriented films deposited on STO and NGO substrates, respectively, and exchanged at 338, 391 and 473 ºC, during 17655, 628 and 4941 s,

respectively. The scheme (in *c*) shows the experimental arrangement for this longitudinal geometry.

Fig. 5. Arrhenius plots of the tracer oxygen surface exchange rate *k**(a) and oxygen tracer diffusivities *D** (b) measured in the longitudinal geometry for the different GBCO film orientations. The graphs include also the values reported for bulk material for comparison.[3] Dashed lines are only a guide to the eye.

Table 1

Cell parameters of GBCO, STO and NGO structures along with calculated mismatch for the different orientations. The table contains also the values of the film cell parameters measured from reciprocal space maps

Substrate cell parameters (Å)	plane cut parameters (Å)	GBCO Area mismatch* (%)	Measured Out-of-plane parameter (Å)	Measured In-plane-parameters (Å)	GBCO orientation
STO *Pm*-3*m* Cubic *a*= 3.905	(001) *a'*=*b'*= 3.905	*ab*: **+0.37** *bc*: +2.3 *ac*: +4.1	3.775	3.8965 (A) 3.925 (B)	*c*-axis
NGO *Pbnm* *Orthorhombic* *a*= 5.43 *b*= 5.50 *c*= 7.71	(110) *a'*= 3.864 *b'*= 3.855	*ab*: -1.99 *bc*: **-0.02** *ac*: +1.85	3.867	3.815 (C) 3.925 (D)	*a*-axis

* calculated from the difference between the area of the corresponding plane of the primitive GBCO cell (Orthorhombic *Pmmm*, *a* = 3.862 Å; *b*/2 = 3.934 Å; *c*/2 = 3.786 Å) and the corresponding substrate.

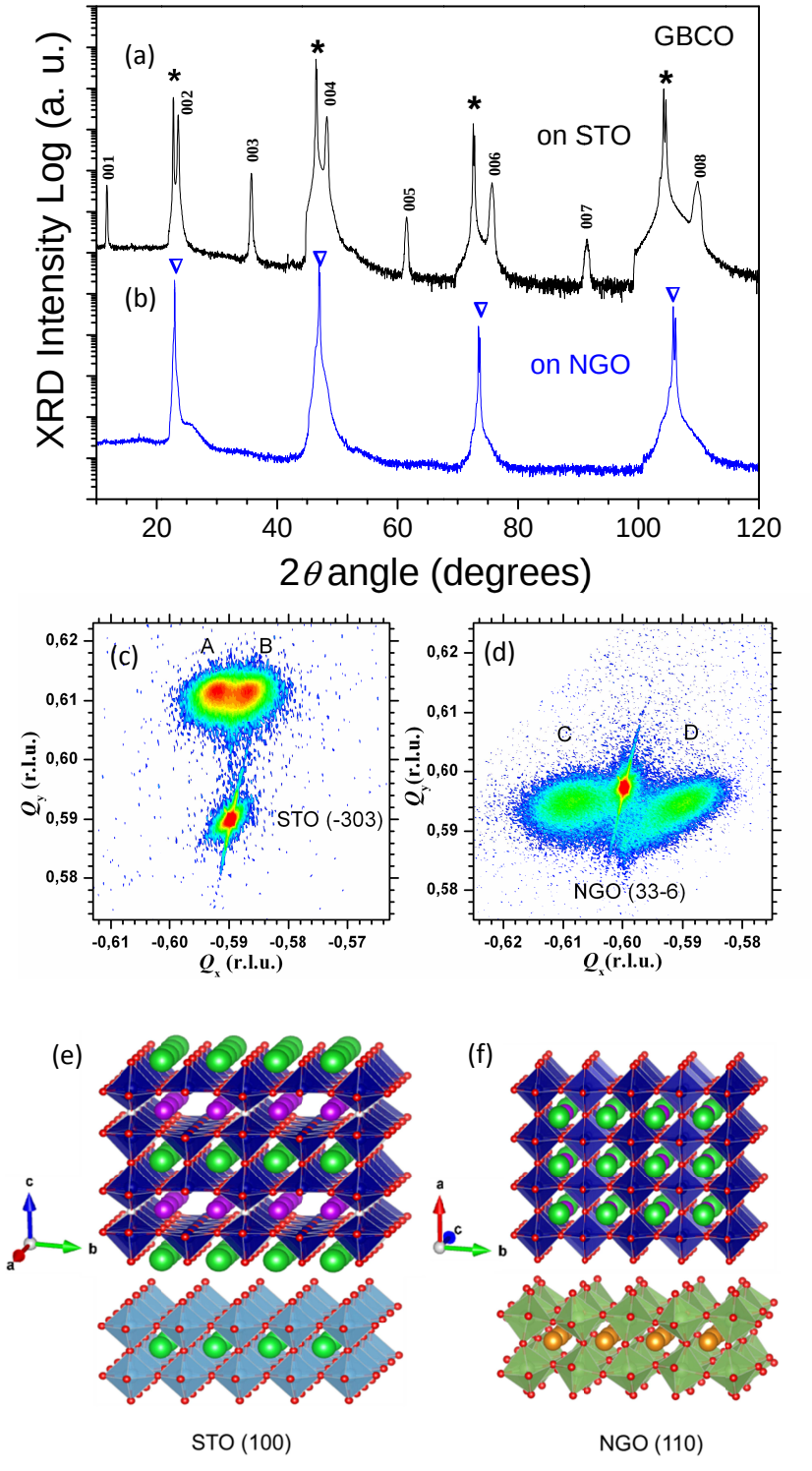
(a)
GBCO
on STO
001
002
003
004
005
006
007
008
(b)
on NGO
XRD Intensity Log (a. u.)
2θ angle (degrees)
(c)
A
B
STO (-303)
(d)
C
D
NGO (33-6)
Q_y (r.l.u.)
Q_x (r.l.u.)
(e)
(f)
STO (100)
NGO (110)

Fig. 1

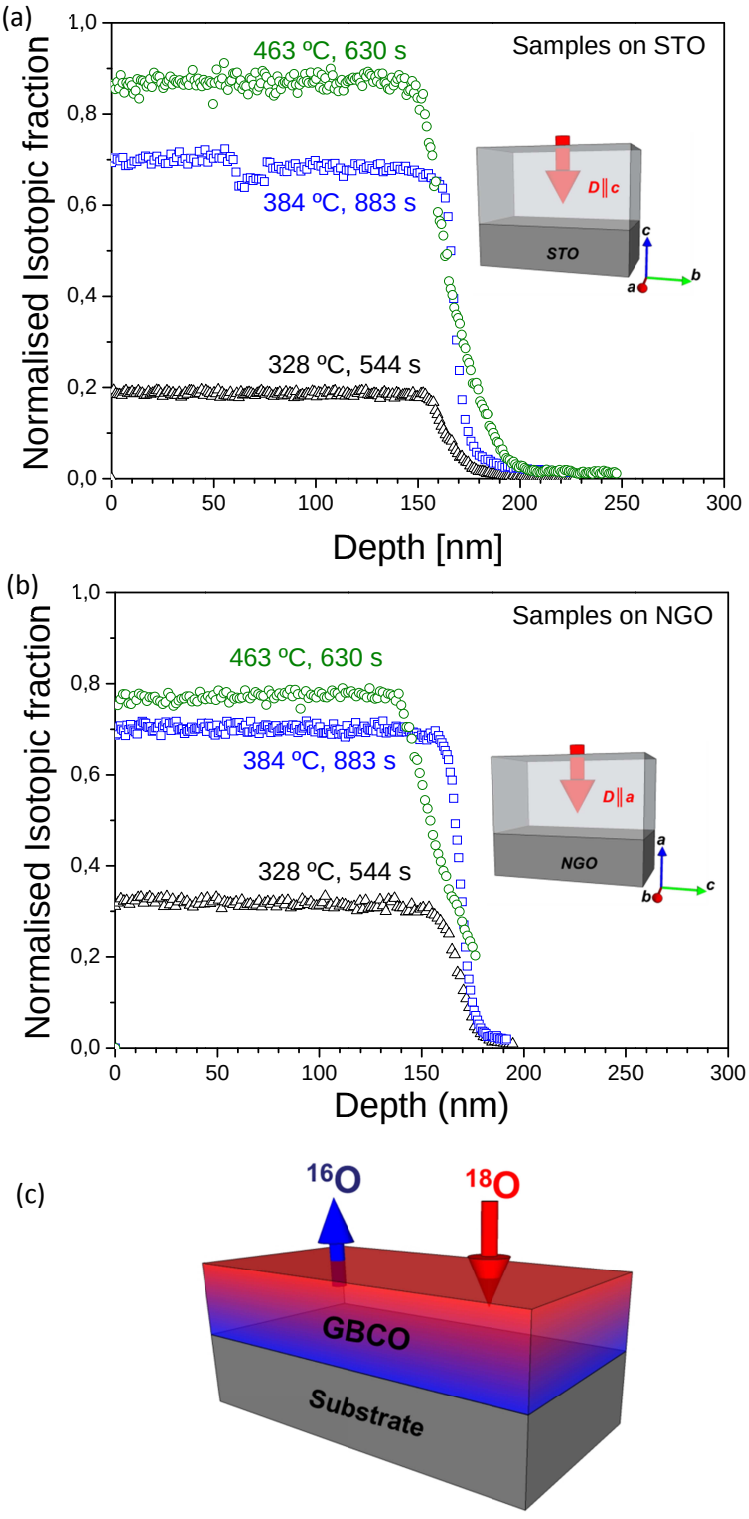
(a)
Normalised Isotopic fraction
Depth [nm]
463 ºC, 630 s
384 ºC, 883 s
328 ºC, 544 s
Samples on STO
D∥c
STO
(b)
Normalised Isotopic fraction
Depth (nm)
463 ºC, 630 s
384 ºC, 883 s
328 ºC, 544 s
Samples on NGO
D∥a
NGO
(c)
16O
18O
GBCO
Substrate

Fig. 2

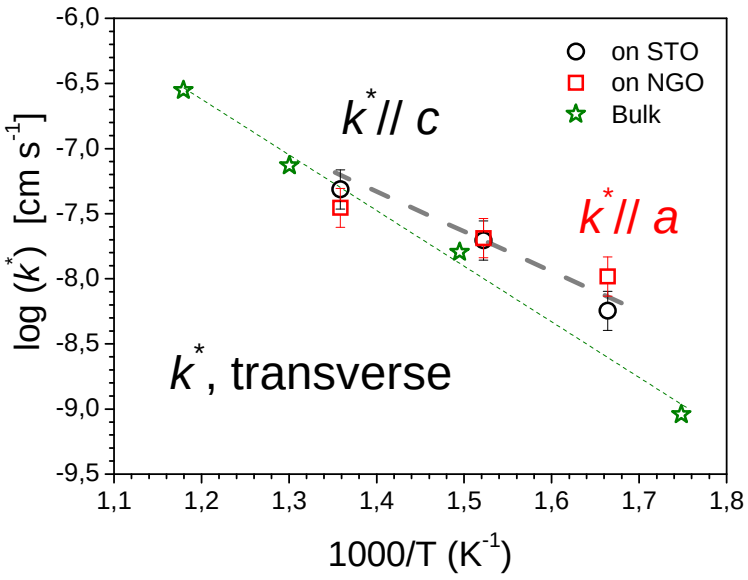
-6,0
-6,5
-7,0
-7,5
-8,0
-8,5
-9,0
-9,5
1,1
1,2
1,3
1,4
1,5
1,6
1,7
1,8
log (k*) [cm s-1]
1000/T (K-1)
on STO
on NGO
Bulk
k*// c
k*// a
k*, transverse

Fig. 3

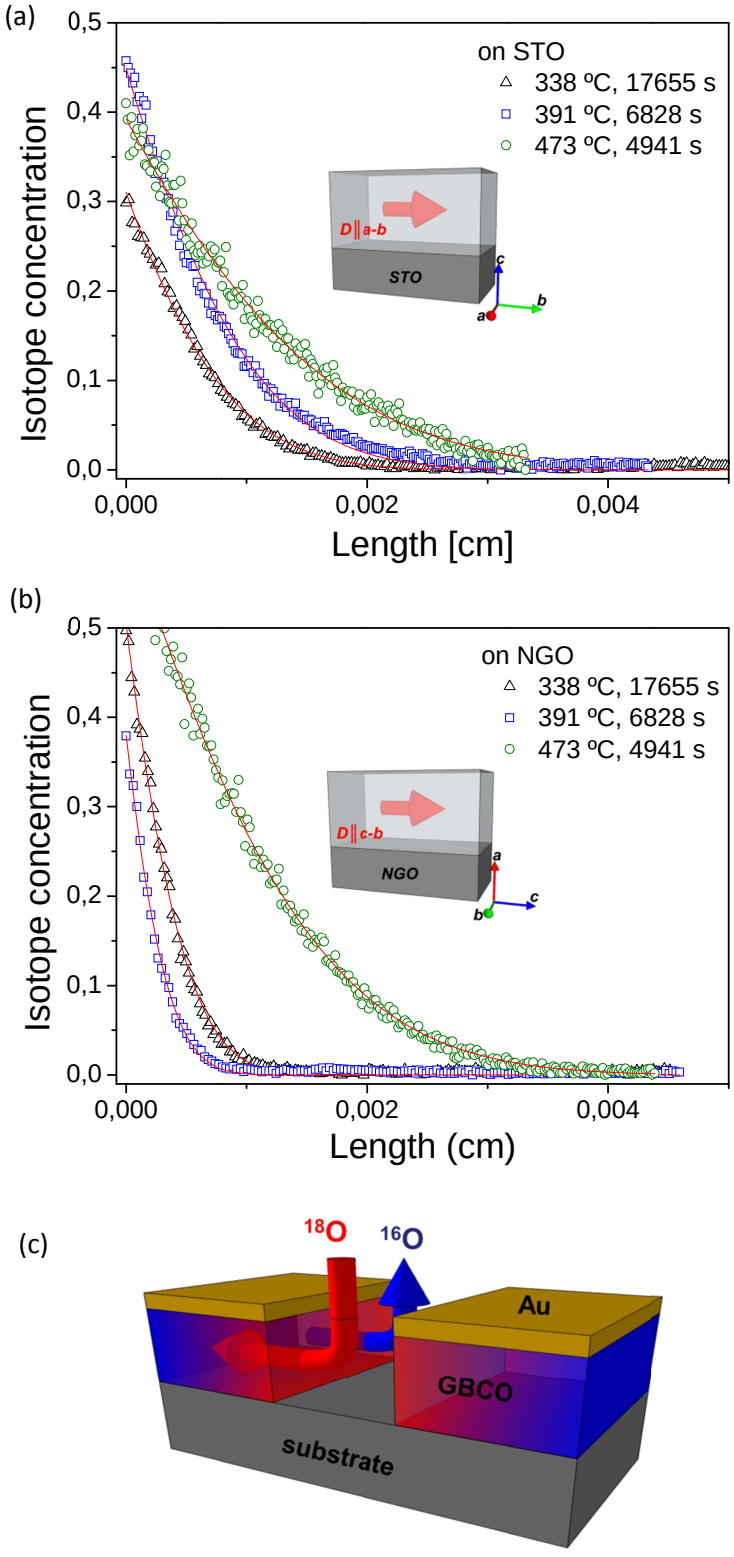
(a)
Isotope concentration
Length [cm]
on STO
338 ºC, 17655 s
391 ºC, 6828 s
473 ºC, 4941 s
D∥a-b
STO
(b)
Isotope concentration
Length (cm)
on NGO
338 ºC, 17655 s
391 ºC, 6828 s
473 ºC, 4941 s
D∥c-b
NGO
(c)
18O
16O
Au
GBCO
substrate

Fig. 4

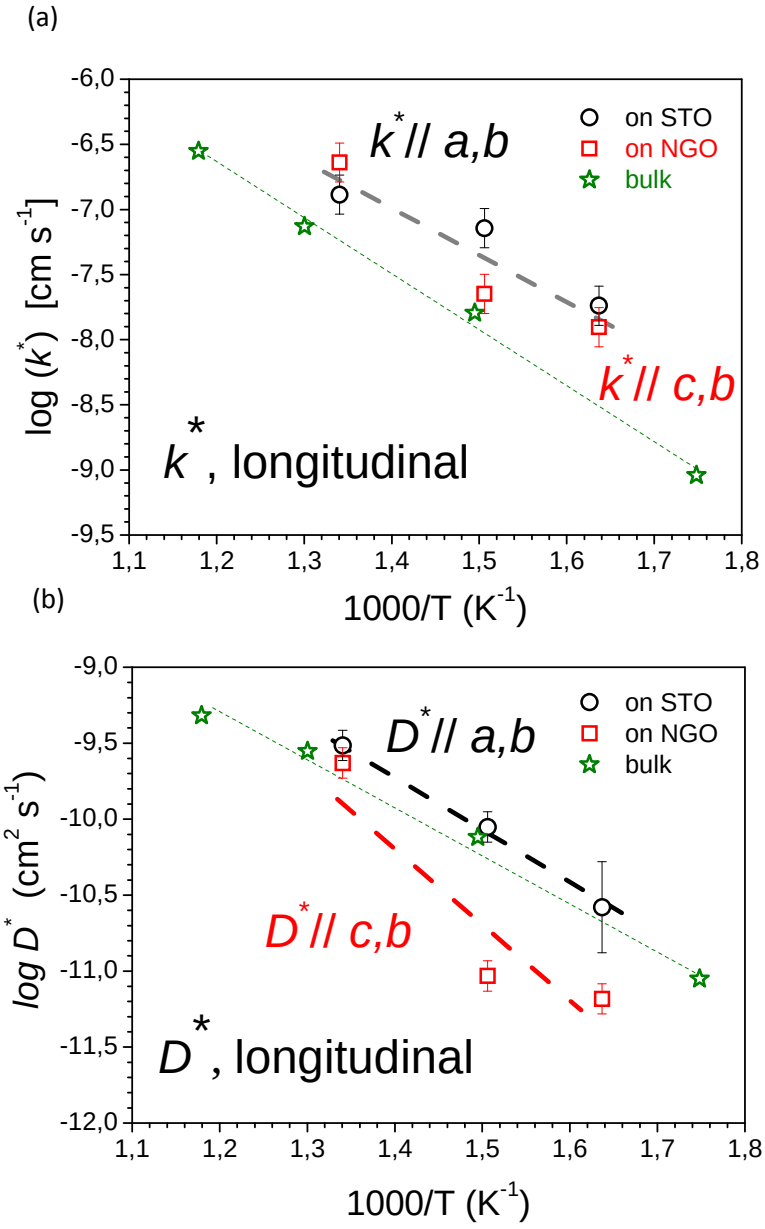
(a)
-6,0
-6,5
-7,0
-7,5
-8,0
-8,5
-9,0
-9,5
log (k*) [cm s-1]
1,1
1,2
1,3
1,4
1,5
1,6
1,7
1,8
1000/T (K-1)
k*// a,b
k*// c,b
k*, longitudinal
on STO
on NGO
bulk
(b)
-9,0
-9,5
-10,0
-10,5
-11,0
-11,5
-12,0
log D* (cm2 s-1)
1,1
1,2
1,3
1,4
1,5
1,6
1,7
1,8
1000/T (K-1)
D*// a,b
D*// c,b
D*, longitudinal
on STO
on NGO
bulk

Fig. 5

Barcelona, Feb 18 2013

Dear Editor,

Please find attached the manuscript that we are submitting to *Journal of Materials Chemistry A* entitled: *"**Anisotropic ^{18}O tracer diffusion in epitaxial films of $GdBaCo_2O_{5+\delta}$ cathode material with different orientations"*** by James Zapata, *et al*.

In the present paper we succeeded in depositing high quality *c*- and *a*-axis oriented epitaxial films of the $GdBaCo_2O_{5+\delta}$ (GBCO) compound with layered perovskite structure, which is currently under consideration as a promising cathode material for Intermediate Temperature Solid Oxide Fuel Cells (IT-SOFCs). These films allowed us to experimentally prove for the first time the anisotropy in the oxygen diffusion *D** in this material, being about one order of magnitude larger along the *a-b* plane in comparison to the diffusion along the *c*-axis direction. Corresponding oxygen surface exchange rates *k** are larger than in reported bulk material, but do not show any anisotropy for *c* - and *a*–axis orientation. These findings are of primary importance for engineering high-performance cathodes based on this compound.
We appreciate very much that you take this paper into consideration for publication in *Journal of Materials Chemistry A*.

Sincerely

Jose Santiso (on behalf of the rest of the authors)

José Santiso jsantiso@cin2.es
Pulsed Laser Deposition and Nanoionics Group
Nanoscience and Nanotechnology Research Centre, CIN2 (CSIC/ICN)
08193 Bellaterra, Barcelona, Spain
Ph: +34 93 5814700